Brief Communication

MOLECULAR METABOLISM

Genetic loss of AMPK-glycogen binding destabilises AMPK and disrupts metabolism

Nolan J. Hoffman [1,*], Jamie Whitfield [1], Natalie R. Janzen [1], Mehdi R. Belhaj [1], Sandra Galic [2], Lisa Murray-Segal [2], William J. Smiles [2], Naomi X.Y. Ling [2], Toby A. Dite [2,6], John W. Scott [1,2,3], Jonathan S. Oakhill [1,2], Robert Brink [4,5], Bruce E. Kemp [1,2,*], John A. Hawley [1,**]**

ABSTRACT

Objective: Glycogen is a major energy reserve in liver and skeletal muscle. The master metabolic regulator AMP-activated protein kinase (AMPK) associates with glycogen via its regulatory β subunit carbohydrate-binding module (CBM). However, the physiological role of AMPK-glycogen binding in energy homeostasis has not been investigated *in vivo*. This study aimed to determine the physiological consequences of disrupting AMPK-glycogen interactions.

Methods: Glycogen binding was disrupted in mice via whole-body knock-in (KI) mutation of either the AMPK β1 (W100A) or β2 (W98A) isoform CBM. Systematic whole-body, tissue and molecular phenotyping was performed in KI and respective wild-type (WT) mice.

Results: While β1 W100A KI did not affect whole-body metabolism or exercise capacity, β2 W98A KI mice displayed increased adiposity and impairments in whole-body glucose handling and maximal exercise capacity relative to WT. These KI mutations resulted in reduced total AMPK protein and kinase activity in liver and skeletal muscle of β1 W100A and β2 W98A, respectively, versus WT mice. β1 W100A mice also displayed loss of fasting-induced liver AMPK total and α-specific kinase activation relative to WT. Destabilisation of AMPK was associated with increased fat deposition in β1 W100A liver and β2 W98A skeletal muscle versus WT.

Conclusions: These results demonstrate that glycogen binding plays critical roles in stabilising AMPK and maintaining cellular, tissue and whole-body energy homeostasis.

Keywords AMP-activated protein kinase; Carbohydrate-binding module; Cellular energy sensing; Exercise; Liver; Skeletal muscle

1. INTRODUCTION

Energy-sensing protein kinases are essential for maintaining metabolic energy homeostasis via integration of intracellular and extracellular nutrient signals to regulate energy mobilisation and storage [1]. The AMP-activated protein kinase (AMPK) is a highly conserved αβγ heterotrimer that senses cellular energy status and functions at the interface of carbohydrate, fat and protein metabolism. AMPK activity is regulated by cellular energy status, whereby decreased energy availability leads to AMPK activation and restoration of energy homeostasis. The AMPK α subunit phosphorylates a range of substrates, including rate-limiting enzymes of key metabolic pathways with regulatory roles in fatty acid, cholesterol and glycogen synthesis. The γ subunit senses adenine nucleotide ratios [2–4], and the β subunit permits its interaction with glycogen through the β1 and β2 subunit carbohydrate-binding modules (CBM) [5,6]. In rodents, AMPK β1 and β2 are predominantly expressed in the major glycogen-storing tissues, liver and skeletal muscle, respectively [7]. *In vitro* studies have demonstrated that glycogen binding depends on a pair of conserved tryptophan residues within the AMPK β1 (W100 and W133) and β2 (W98 and W133) CBMs, respectively. Mutating a single tryptophan in the pair (i.e., β1 W100 or the analogous β2 W98) is sufficient to abolish AMPK-glycogen binding *in vitro* [5].

Glycogen storage is concurrently regulated by AMPK activity to help meet cellular and whole-body energy demands, and research over the past two decades has provided molecular, cellular and physiological

[1]Exercise and Nutrition Research Program, Mary MacKillop Institute for Health Research, Australian Catholic University, Level 5, 215 Spring Street, Melbourne, Victoria 3000, Australia [2]St. Vincent's Institute of Medical Research and Department of Medicine, University of Melbourne, 9 Princes Street, Fitzroy, Victoria 3065, Australia [3]The Florey Institute of Neuroscience and Mental Health, 30 Royal Parade, Parkville, Victoria 3052, Australia [4]Immunology Division, Garvan Institute of Medical Research, 384 Victoria Street, Darlinghurst, New South Wales 2010, Australia [5]St. Vincent's Clinical School, UNSW Sydney, Level 5 deLacy Building, St. Vincent's Hospital, Darlinghurst, New South Wales 2010, Australia

[6] Present Address: Medical Research Council Protein Phosphorylation and Ubiquitylation Unit, School of Life Sciences, University of Dundee, Dundee DD1 5EH United Kingdom.

*Corresponding author. E-mail: nolan.hoffman@acu.edu.au (N.J. Hoffman).

**Corresponding author. E-mail: john.hawley@acu.edu.au (J.A. Hawley).

***Corresponding author. St. Vincent's Institute of Medical Research and Department of Medicine, University of Melbourne, 9 Princes Street, Fitzroy, Victoria 3065, Australia. E-mail: bkemp@svi.edu.au (B.E. Kemp).

Received May 25, 2020 • Revision received June 9, 2020 • Accepted June 25, 2020 • Available online 29 June 2020

https://doi.org/10.1016/j.molmet.2020.101048

evidence of interactive roles for AMPK and glycogen [8]. Several lines of *in vivo* and *in vitro* evidence suggest that glycogen may have an inhibitory effect on AMPK. For example, activation of AMPK *in vivo* is suppressed in glycogen replete compared to glycogen depleted skeletal muscle in response to AICAR perfusion [9] and muscle contraction [10] in rats and exercise stimulation in humans [11,12]. In addition, both glycogen and single α 1−6 branch chain oligosaccharides have been reported to inhibit AMPK activity *in vitro* [13]. However, results from other *in vitro* studies reveal no evidence of inhibition of AMPK activity by glycogen [5,14]. Furthermore, the physiological role of AMPK-glycogen binding has not been directly investigated *in vivo*.

To determine the physiological consequences of disrupting AMPK β1 and β2 glycogen binding, we generated whole-body AMPK knock-in (KI) mice in which the tryptophan residues mediating glycogen binding in the AMPK β1 or β2 subunit isoforms were mutated to alanine. Based on reports of AMPK inhibition by glycogen, we hypothesised that genetic loss of AMPK β1 or β2 glycogen binding in mice would increase liver and skeletal muscle AMPK activity, respectively. Utilising these two AMPK KI models and focusing on liver and skeletal muscle as two primary glycogen-storing tissues, we performed systematic phenotyping with the aim of determining isoform-specific whole-body, tissue and molecular consequences of disrupting AMPK-glycogen binding *in vivo*.

2. MATERIALS AND METHODS

2.1. Animal models

All mouse procedures were performed with the approval of the St. Vincent's Hospital (Melbourne, Australia) Animal Ethics Committee (AEC 025−15 and 011−19), conforming to all the requirements of the National Health and Medical Research Council of Australia (NHMRC) and in accordance with the Australian code of practice for the care and use of animals for scientific purposes (8th Edition 2013) and the National Institutes of Health Guide for the Care and Use of Laboratory Animals (NIH Publications No. 8023, revised 1978). Wild-type (WT) and KI mice were group-housed (2−5 per cage) in pathogen-free microisolator cages and maintained on 12:12-h light−dark cycles with controlled temperature (21 °C), humidity, bedding for environmental enrichment and *ad libitum* access to water and standard rodent chow diet (6% fat, 20% protein and 29% starch, Barastoc, Ridley Agriproducts, Pakenham, VIC, Australia). For all experiments, sample sizes indicate the number of distinct male WT and KI mice or distinct tissue samples from mice that were age-matched within two weeks of age and randomised to respective experimental groups.

Prkab1^{W100A} (β1 W100A) and *Prkab2*^{W98A} (β2 W98A) KI mice were produced by the Mouse Engineering Garvan/ABR (MEGA) Facility using CRISPR/Cas9 gene targeting in C57BL/6J mouse embryos following established molecular and animal husbandry techniques [15]. Single guide RNAs (sgRNA) were based on target sites in exon 3 of *Prkab1* (AGATCCTTACCTTCTCGTGA*GGG*) and *Prkab2* (CTTGGTGCTCCAATTGTTGA*AGG*) (protospacer-associated motif [PAM] italicised and underlined). In each case, the specific sgRNA (15 ng/μl) was microinjected into the nucleus and cytoplasm of C57BL/6J zygotes together with polyadenylated *Streptococcus* (*S.*) *pyogenes* Cas9 mRNA (30 ng/μl) and a gene-specific 150 base single-stranded, anti-sense, deoxy-oligonucleotide homologous recombination substrate (15 ng/μl). For *Prkab1,* the oligonucleotide encoded the W100A (TGG > GCG) substitution plus a PAM-inactivating silent mutation in the P104 codon (CCC > CCA) (Supplementary Fig 1), while for *Prkab2,* the oligonucleotide encoded the W98A (TGG > GCG) substitution plus a PAM-inactivating silent mutation in the S94 codon (TCC > TCA) (Supplementary Fig 1). Founder males heterozygous for alleles that had been successfully modified by homologous recombination were backcrossed with C57BL/6J females for several generations to establish the *Prkab1*^{W100A} and *Prkab2*^{W98A} KI lines before experiments were commenced. Breeding was performed on homozygous carriers of each KI mutation, and KI and WT breeders were annually backcrossed to generate heterozygous carriers used to rederive homozygous KI mice used in breeding.

Confirmatory genotyping was performed from tail samples by TransnetYX (Cordova, TN, USA). Male and female mice aged 12−14 weeks old from each WT and KI genotype (4 from each sex and genotype) were analysed by the Australian Phenomics Network Histopathology and Organ Pathology Service at the University of Melbourne at the commencement of the study, and no overt pathology was observed to be associated with KI mutation in either sex or genotype. For subsequent physiological and metabolic characterisation, only male mice were investigated due to limitations in age-matched mouse cohort availability and to ensure sufficient female mice from each genotype were available to maintain breeding colonies. Mice were euthanised via cervical dislocation, and tissues were dissected rapidly from age-matched mice in the fed state at 0800 h, unless otherwise stated. Following excision, tissues were immediately snap-frozen, placed in liquid nitrogen and stored at −80 °C for subsequent analysis.

2.2. Reagents

2.2.1. Glucose and insulin tolerance testing

Intraperitoneal glucose (IPGTT) and insulin tolerance testing (IPITT) were performed in 10−16-wk-old male age-matched mice, respectively, with ≥1 wk of recovery between tests. Mice were fasted for 6 h, commencing at 0800 h before either glucose (1 g/kg total body mass, or total lean mass where indicated; Sigma−Aldrich, St. Louis, MO, USA) or insulin (0.5 units/kg total body mass; Humulin, Eli Lilly and Company, Indianapolis, IN, USA) was injected intraperitoneally. Glucose and insulin doses were selected to detect subtle differences between genotypes. Glucose concentration was measured from tail blood samples (Accu-Check Performa, Roche Diagnostics GmbH, Mannheim, Germany), and area under the curve (AUC) for IPGTT and IPITT was analysed using GraphPad Prism (v8, GraphPad Software, La Jolla, CA, USA).

2.2.2. Body composition and tissue fat and glycogen measurements

Body composition was assessed in 8−15-wk-old male age-matched WT and KI mice by nuclear magnetic resonance imaging using the EchoMRI Body Composition Analysis 3-in-1 system (EchoMRI, Houston, TX, USA). For tissue fat measurements, a small portion (150−250 mg) of freshly isolated liver or quadriceps muscle (selected to ensure sufficient snap-frozen gastrocnemius muscle remaining for subsequent analyses) was weighed and analysed via EchoMRI. For tissue glycogen measurements, liver and gastrocnemius muscles from fed and overnight fasted mice were dissected, snap-frozen, freeze-dried and powdered. An aliquot of freeze-dried liver or gastrocnemius muscle (2−3 mg) was used to determine tissue glycogen content as previously described [16].

2.2.3. Metabolic caging

Metabolic caging was performed using the Comprehensive Lab Animal Monitoring System (CLAMS; Columbus Instruments, Columbus, OH, USA). Mice were singly housed at 21 °C and food intake, infrared−based activity, O_2/CO_2 consumption and indirect calorimetry was

continuously measured for 60 h after 6 h of acclimatisation in the CLAMS. Data for each cage was collected every 16–18 min. Hourly, dark/light cycle and 24-h averages were calculated following acclimatisation. Fat and carbohydrate oxidation and total energy expenditure were calculated as described previously [17].

2.2.4. Treadmill exercise testing

Following 4 days of treadmill acclimatisation, mice completed an incremental maximal exercise capacity test at 0° incline on an Exer3/6 rodent treadmill (Columbus Instruments, Columbus, OH, USA). Mice rested on the treadmill for 15 min on day 1 of acclimatisation, followed by running for 5 min at 5 m/min on day 2 and 5 min at 10 m/min on day 3. On day 4, mice ran for 5 min at 10 m/min, 12 m/min for 5 min, then 15 m/min for 5 min. For maximal exercise capacity testing on day 5, mice ran in the fed state for 2 min at 10 m/min at 0° incline, increasing speed by 1 m/min every 2 min until exhaustion, defined as the inability to compel the mouse to remain running despite continued manual prodding using a bottle brush. For assessment of skeletal muscle exercise signalling, mice were subjected to maximal exercise capacity treadmill testing at 5° incline after acclimatisation. After 2–3 days of rest, mice underwent submaximal exercise testing in the fed state at 70% of maximal running speed at 0° incline until exhaustion.

2.2.5. Serum analysis

Whole blood samples (100 μl) were collected via retro-orbital bleeding into non-coated polypropylene tubes and left to clot at room temperature for 15–30 min, followed by centrifugation at 1,000 *g* for 10 min at 4 °C. Serum supernatant was aliquoted to prevent freeze–thaw cycles and stored at −80 °C. Hormone and lipid concentrations were determined from 5-μl serum aliquots using Ultra Sensitive Mouse Insulin ELISA kits (Crystal Chem, Elk Grove Village, IL, USA; 90080), non-esterified fatty acid (NEFA)-C colorimetric assays (Wako Pure Chemical Industries, Osaka, Japan; 279–75401) and triglyceride (TG) colorimetric assays (Abcam, Cambridge, United Kingdom; ab65336) according to each manufacturer's instructions.

2.2.6. Protein analysis

Liver, gastrocnemius skeletal muscle and adipose tissue samples were excised from mice, immediately snap-frozen using freeze clamps, placed in liquid nitrogen and stored at −80 °C until analysis. To generate whole liver, muscle and adipose tissue lysates, 40 mg of frozen tissue was homogenised in lysis buffer containing 50 mM of Tris.HCl (pH 7.5), 1 mM of EDTA, 1 mM of EGTA, 10% glycerol, 1% Triton X-100, 50 mM of sodium fluoride, 5 mM of sodium pyrophosphate, 1 mM of DTT, 10 μg/ml of trypsin inhibitor, 2 μg/ml of aprotinin, 1 mM of benzamidine, and 1 mM of PMSF. Samples were centrifuged at 16,000 *g* for 30 min at 4 °C to remove cellular debris, and protein concentration was determined via bicinchoninic acid (BCA) protein assay (Pierce, Rockford, IL, USA; 23,227). Lysates were resuspended in Laemmli sample buffer, and 10 μg of protein from each sample was loaded into precast 4–20% or 4–15% Mini-Protean TGX Stain-Free Protein Gels (Bio-Rad, Hercules, CA, USA; 4568094 [10-well] or 4568086 [15-well]). After electrophoresis, gels were activated according to the manufacturer's instructions (Chemidoc MP Imaging System; Bio-Rad, Hercules, CA, USA) and transferred to Immobilon-P PVDF membranes (Merck Millipore, Burlington, MA, USA). A stain-free image of each membrane was obtained for protein loading normalisation before blocking for 1 h with 5% skim milk powder, washing (3 × 5 min) with 10 mM of Tris.HCl, 100 mM of NaCl and 0.1% Tween 20 solution (TBS-T) and incubating with primary antibody diluted in 2.5% bovine serum albumin (BSA) in TBS-T (1:1,000; except rodent OXPHOS cocktail antibody that was diluted 1:250) overnight at 4 °C with rocking. Following washing, membranes were incubated for 1 h with secondary antibody diluted in TBS-T (1:2,000). Proteins were detected via enhanced chemiluminescence (ECL) using SuperSignal West Femto Maximum Sensitivity Substrate (Life Technologies, Carlsbad, CA, USA; 34,096) and Bio-Rad ChemiDoc MP Imaging System (Hercules, CA, USA).

Antibodies against total ACC (3662), phospho-ACC Ser79 (3661), total AMPK α (2532), total AMPK β1/β2 (4150; clone 57C12; RRID: AB_10828832), phospho-AMPK Thr172 (2531), CPT1a (12252; clone D3B3), GAPDH (2118; clone 14C10; RRID: AB_561053), Glycogen Synthase (GS; 3886; clone 15B1; RRID:AB_2116392), GS p-S641 (47043; clone D4H1B) and horseradish peroxidase (HRP)-linked anti-rabbit (7074; RRID: AB_2099233) and anti-mouse (7076; RRID: AB_330924) immunoglobulin G (IgG) secondary antibodies were purchased from Cell Signaling Technology (Danvers, MA, USA). CPT1b (ab134988), citrate synthase (ab96600; RRID: AB_10678258), total OXPHOS rodent antibody cocktail (ab110413; RRID: AB_2629281) and VDAC1 (ab14734; RRID: AB_443084) were purchased from Abcam (Cambridge, United Kingdom). The volume density of each target band was quantified using Bio-Rad Image Lab v4 and normalised to total protein in each lane using stain-free imaging technology (Bio-Rad, Hercules, CA, USA). For the rodent OXPHOS cocktail antibody, protein loading was also determined using GAPDH imaged from the same membrane after application of Restore PLUS Western blot stripping buffer (Thermo Fisher Scientific, Waltham, MA, USA; 46430). Following protein loading normalisation, each phosphoprotein was normalised to respective total protein.

2.2.7. Nucleotide measurements

Adenine nucleotides were measured in excised and snap-frozen liver and gastrocnemius muscle by liquid chromatography mass spectrometry (LC-MS) using an AB SCIEX 5500 QTRAP mass spectrometer (Framingham, MA, USA) as previously described [18]. Adenylate energy charge (AEC) was calculated from ratios of [AMP], [ADP] and [ATP] using the following equation: $AEC = ([ATP] + (0.5[ADP]))/([ATP] + [ADP] + [AMP])$.

2.2.8. AMPK-glycogen binding assay

Bacterially expressed WT AMPK (75 μg α1β1γ1) and 75 μg of either β1 W100A (α1β1[W100A]γ1) or β2 W98A (α1β2[human W99A; orthologous to mouse W98A]γ1) were purified as previously described [19] and incubated with 1.5% (w/v) bovine liver glycogen, type IX (Sigma–Aldrich, St. Louis, MO, USA; G0885) in a total volume of 1 ml of phosphate-buffered saline (PBS) and 0.1% NP-40 for 60 min at 4 °C with rotation, followed by centrifugation at 200,000 *g* for 60 min at 4 °C [5]. After centrifugation, the glycogen pellet was washed with PBS prior to resuspension in Laemmli sample buffer and immunoblotting (detailed above).

2.2.9. AMPK immunoprecipitation and activity assays

AMPK α was immunoprecipitated (IP) from 30 mg of excised and clamp frozen liver or gastrocnemius muscle. Briefly, tissues were homogenised in ice-cold lysis buffer (10 μl buffer per mg tissue wet weight; 50 mM of Tris.HCl [pH = 7.4], 150 mM of NaCl, 50 mM of NaF, 1 mM of NaPPi, 1 mM of EDTA, 1 mM of EGTA, 1 mM of DTT, 1% [v/v] Triton X-100). Cellular debris was removed by centrifugation at 13,000 *g* for 15 min, and protein concentrations were determined using the BCA assay. AMPK α was IP from 750 μg of WT, 1.5 mg of β1 W100A or 1.5 mg of β2 W98A lysate to balance total AMPK α in each

WT and KI reaction containing 40 μl of a 50% slurry of Protein A agarose fast flow beads (Sigma–Aldrich, St. Louis, MO, USA; P3476) pre-complexed with an AMPK pan-α antibody [20] for 1.5 h at 4 °C with mixing (5 μl of antibody per 20 μl of pre-equilibrated beads in each reaction).

Following IP, beads were washed three times in lysis buffer (10% glycerol, 50 mM of Tris.HCl [pH = 7.4], 150 mM of NaCl, 50 mM of NaF, 1 mM of NaPPi, 1 mM of EGTA, 1% [v/v] Triton X-100) and resuspended in 20 μl of activity assay buffer (50 mM of HEPES [pH = 7.4], 1 mM of DTT, 0.01% [v/v] Tween-20). Half of the beads were used to determine AMPK activity by phosphorylation of the SAMS peptide using 100 μM of SAMS, 200 μM of [γ-^{32}P]ATP (Perkin Elmer, Waltham, MA, USA) and 5 mM of $MgCl_2$ in a standard 25-μl volume assay performed with agitation at 30 °C. Reactions were terminated after 10 min by spotting 15-μl aliquots of the reaction mixture onto P81 phosphocellulose paper (Whatman, Maidstone, UK; WHA-3698-915) and washing in 1% phosphoric acid. An aliquot of whole cell lysate and the remaining bead solution was resuspended in Laemmli sample buffer prior to immunoblotting as described above. Radioactivity was quantified by scintillation counting, and samples were adjusted for equal lysate protein input to calculate tissue total AMPK α activity (Figure 4Q,S). To calculate AMPK α-specific activity, total AMPK α activity was divided by the AMPK α signal determined by immunoblot analysis of each IP sample (Figure 4R,T), which was calculated by densitometry (Figure 4O,P bottom panels) relative to 100 ng of bacterially expressed, purified AMPK α protein loaded on each gel.

2.2.10. RNA extraction and gene expression analysis

RNA was extracted using TRIzol LS Reagent (Life Technologies, Carlsbad, CA, USA; 10296028) from 35 mg of excised and freeze-clamped liver and gastrocnemius muscle collected from age-matched mice in the fed, rested state. Between 400 and 1,000 ng of RNA was treated with Amplification Grade DNase I (Invitrogen, Carlsbad, CA, USA; 18068–015) and reverse-transcribed using a SuperScript VILO cDNA Synthesis Kit (Life Technologies, Carlsbad, CA, USA; 11754–050). Pre-amplification was performed using TaqMan Custom PreAmp Pool and PreAmp Master Mix (Applied Biosystems, Foster City, CA, USA; 4485255 and 4384266, respectively), and quantitative polymerase chain reaction (qPCR) was performed with a Bio-Rad CFX Connect Real-Time System. Gene expression was normalised to GAPDH using TaqMan Fast Advanced Master Mix (Applied Biosystems; 4444557). The following TaqMan Gene Expression Assays (Applied Biosystems) were used: *Prkab1* (liver, AMPK β1; Mm01201921_m1), *Prkab2* (muscle, AMPK β2; Mm01257133_m1) and *Gapdh* (liver and muscle; Mm99999915_g1). Relative levels of mRNA were assessed using the ΔΔCt method.

2.3. Statistics

Statistical analyses were performed using GraphPad Prism (v8, GraphPad Software, La Jolla, CA, USA). Two-tailed Student's *t* testing was used to detect genotype differences between WT and respective KI mice. Two-way analysis of variance (ANOVA) was used to detect differences between WT and respective KI mice over time or condition with Bonferroni post-hoc testing for multiple comparisons. A mixed-effects model was used to detect differences between fed and fasted glycogen content from WT and respective KI mice with Bonferroni post-hoc testing for multiple comparisons. Values of $P < 0.05$ were considered statistically significant, and all error bars represent mean ± standard error of the mean (SEM).

3. RESULTS

3.1. AMPK β1 and β2 KI mice were generated to determine the roles of glycogen binding *in vivo*

Two whole-body AMPK KI mouse models were generated on a C57BL/6J background using CRISPR/Cas9 gene targeting. Analogous tryptophan residues within either the AMPK β1 (*Prkab1*^{W100A}) or AMPK β2 (*Prkab2*^{W98A}; Supplementary Fig 1) subunit CBM that mediate glycogen binding were mutated to alanine residues. Considering predominant expression of AMPK β1 and β2 in rodent liver and skeletal muscle, respectively [7], these KI models permit *in vivo* interrogation of the metabolic consequences of disrupting AMPK-glycogen binding in these primary glycogen-storing tissues relative to WT mice (Figure 1A).

To confirm that the AMPK β subunit KI mutation reduced glycogen binding, bovine liver glycogen was pelleted via ultracentrifugation in the presence of bacterially expressed WT AMPK or AMPK containing either the β1 W100A or β2 W99A mutation (Figure 1B), orthologous to mouse β2 W98A. We next performed whole-body, tissue and molecular phenotyping using the AMPK KI models to pinpoint isoform-specific consequences of disrupting either AMPK β1 or β2 glycogen binding on AMPK functionality and metabolism. Because these KI lines were genetically distinct and analysed in separate experiments, data from AMPK β1 W100A and β2 W98A KI mice and respective age-matched WT controls are described separately below.

3.2. Disrupting AMPK β2 glycogen binding alters whole-body glucose handling

To first determine whether loss of AMPK-glycogen interaction translated to physiological effects on whole-body metabolism, IPGTT and IPITT were performed in β1 W100A, β2 W98A and respective WT mice. IPGTT uncovered no differences in β1 W100A fasting blood glucose (0 min), blood glucose handling over 120 min post-injection (Figure 1C) or area under the curve (AUC) relative to WT (Figure 1C inset). In contrast, β2 W98A mice displayed normal fasting blood glucose (0 min) but impaired glucose handling (Figure 1D), as determined by increased IPGTT AUC versus WT mice ($P = 0.0290$; Figure 1D inset). There were no associated changes in total body mass (Figure 1E,G) or serum insulin in the fed state (Figure 1F,H) between β1 W100A or β2 W98A and respective WT mice. β1 W100A mice displayed reduced nose to tail tip length ($P = 0.0234$; Supplementary Fig 2), while β2 W98A were comparable to WT (Supplementary Fig 2).

IPITT revealed no differences in blood glucose responses over 120 min post-injection or AUC between β1 W100A (Figure 1I and inset) or β2 W98A (Figure 1J and inset) relative to WT mice. IPGTT increased serum insulin concentration after 20 min (Figure 1K) in both WT ($P = 0.0029$) and β2 W98A mice ($P = 0.0128$) relative to the semi-fasted state at 0 min (overall condition effect $P < 0.0001$), with no overall genotype effect detected ($P = 0.1166$). When IPGTT was performed in WT and β2 W98A mice relative to total lean mass, β2 W98A mice still displayed impaired glucose handling relative to total lean mass (Figure 1L), as determined by increased IPGTT AUC versus WT mice ($P = 0.0409$; Figure 1L inset).

3.3. Disrupting AMPK β2 glycogen binding increases adiposity independent of changes in food intake, physical activity and patterns of whole-body fuel utilisation

β1 W100A mice displayed no changes in absolute fat mass (Figure 2A) or fat mass relative to total body mass (Supplementary Fig 2) versus WT. β1 W100A absolute lean mass was increased relative to WT ($P = 0.0258$; Figure 2B), with no changes observed in lean mass relative to total body mass (Supplementary Fig 2). In contrast, β2

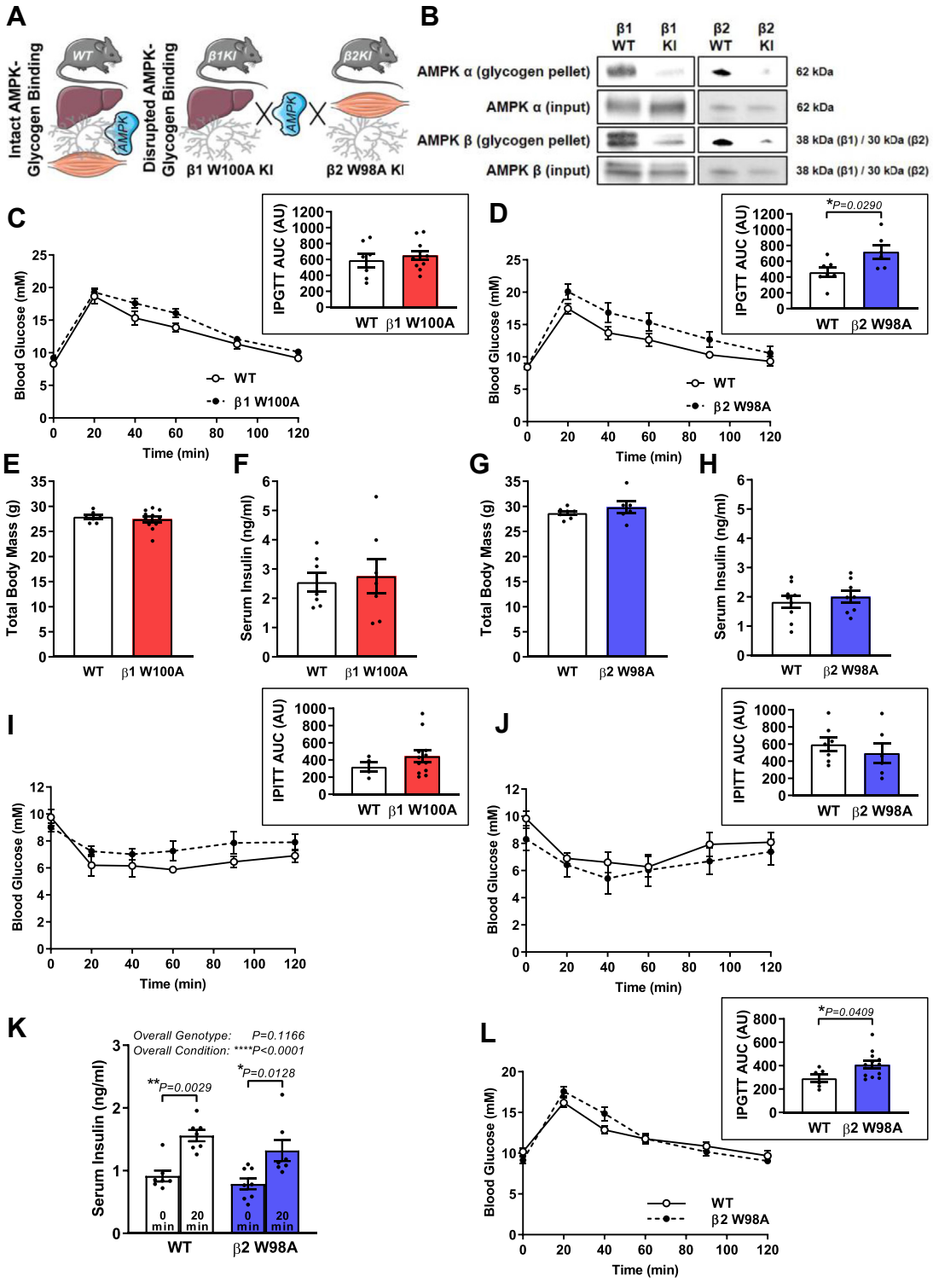

Figure 1: Disrupting AMPK β2 glycogen binding *in vivo* via KI mutation alters whole-body glucose handling. (**A**) Schematic depicts disruption of AMPK-glycogen binding in whole-body KI mice via mutation of the AMPK β1 subunit (W100A) and β2 subunit (W98A), predominantly expressed in liver and skeletal muscle, respectively. (**B**) Association of AMPK α (top panels) and AMPK β (bottom panels) from bacterially expressed AMPK containing β1 KI, β2 KI or respective WT with bovine liver glycogen relative to input protein (representative blots shown from 3 replicate experiments). Following 6-h fast, respective male WT and β1 W100A (**C**; n = 7–11) or β2 W98A (**D**; n = 6–7) age-matched mice (10–16 wk) were subjected to IPGTT (1 g/kg total body mass), and AUC was analysed (**insets**). (**E**) Total body mass (n = 7–11) and (**F**) serum insulin (n = 7) from WT and β1 W100A, or WT and β2 W98A (**G**) total body mass (n = 6–7) and (**H**) serum insulin (n = 8–9) was determined. Following 6-h fast, respective male WT and (**I**) β1 W100A (n = 4–12) or (**J**) β2 W98A (n = 6–7) age-matched mice (12–14 wk) were subjected to IPITT (0.5 units/kg total body mass) and AUC was analysed (**insets**). (**K**) Serum insulin was determined in male age-matched WT and β2 W98A mice (n = 7–8; 12–16 wk) at 0 min and 20 min following IP injection with 1 g/kg total body mass. Following a 6-h fast, male WT and β2 W98A age-matched mice (**L**; n = 6–12; 12–15 wk) were subjected to IPGTT (1 g/kg lean body mass), and AUC was analysed (**inset**). See also Figure S1. Data are represented as mean ± SEM; $*P < 0.05$; $**P < 0.01$; $****P < 0.0001$.

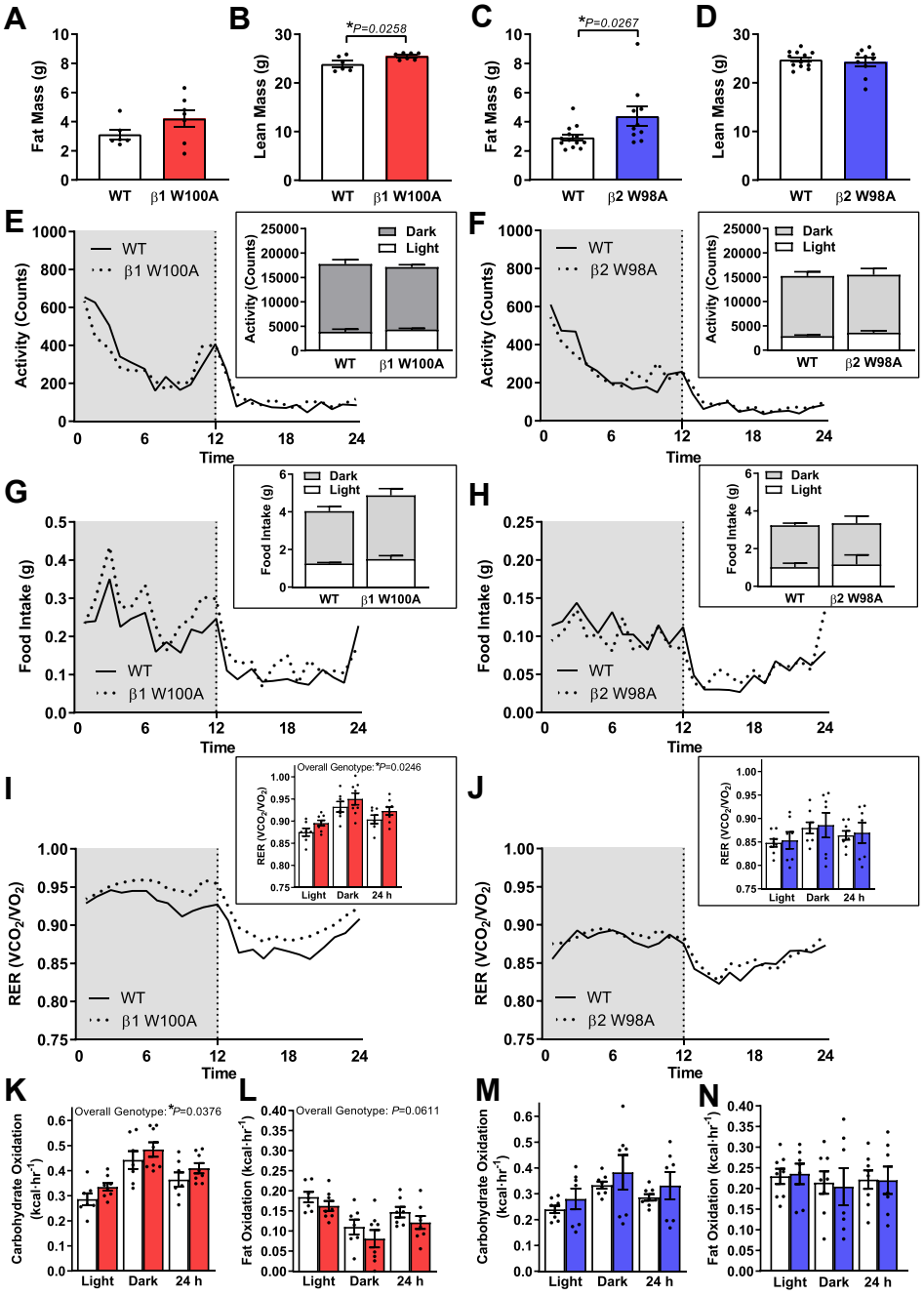

Figure 2: Disrupting AMPK β2 glycogen binding increases adiposity independent of changes in food intake, physical activity or patterns of whole-body fuel utilisation. Male age-matched mice (8–15 wk) were subjected to EchoMRI and CLAMS analyses. (**A**) Absolute fat and (**b**) absolute lean mass for WT and β1 W100A (n = 6–7) and WT and β2 W98A (**C**) absolute fat and (**D**) absolute lean mass (n = 10–13) are shown. (**E**) Infrared-based activity, (**G**) food intake and (**I**) RER (VO_2/VCO_2) were measured in WT and β1 W100A mice (n = 7–8). (**F**) Infrared-based activity, (**H**) food intake and (**J**) RER (VO_2/VCO_2) were measured in WT and β2 W98A mice (n = 7–8). Carbohydrate and fat oxidation were determined using RER from respective WT and β1 W100A (**K and L**; n = 7–8) or β2 W98A (**M and N**; n = 7–8) mice. See also Figure S2. Data are represented as mean ± SEM; $^*P < 0.05$.

W98A mice displayed increases in both absolute fat mass ($P = 0.0267$; Figure 2C) and fat mass relative to total body mass versus WT ($P = 0.0251$; Supplementary Fig 2). No change in absolute lean mass was observed in β2 W98A mice (Figure 2D), despite a reduction in lean mass relative to total mass ($P = 0.0097$; Supplementary Fig 2) versus WT. To interrogate potential explanations for these isoform-specific differences in whole-body glucose handling and body composition, mice were next subjected to metabolic caging. Overall genotype effects were observed for increased respiratory exchange ratio (RER; $P = 0.0246$; Figure 2I) and carbohydrate oxidation ($P = 0.0376$; Figure 2K) in β1 W100A mice versus WT, while the observed trend for an overall genotype effect of decreased fat oxidation in β1 W100A versus WT mice did not reach statistical significance (P = 0.0611; Figure 2L). Post-hoc testing for multiple comparisons

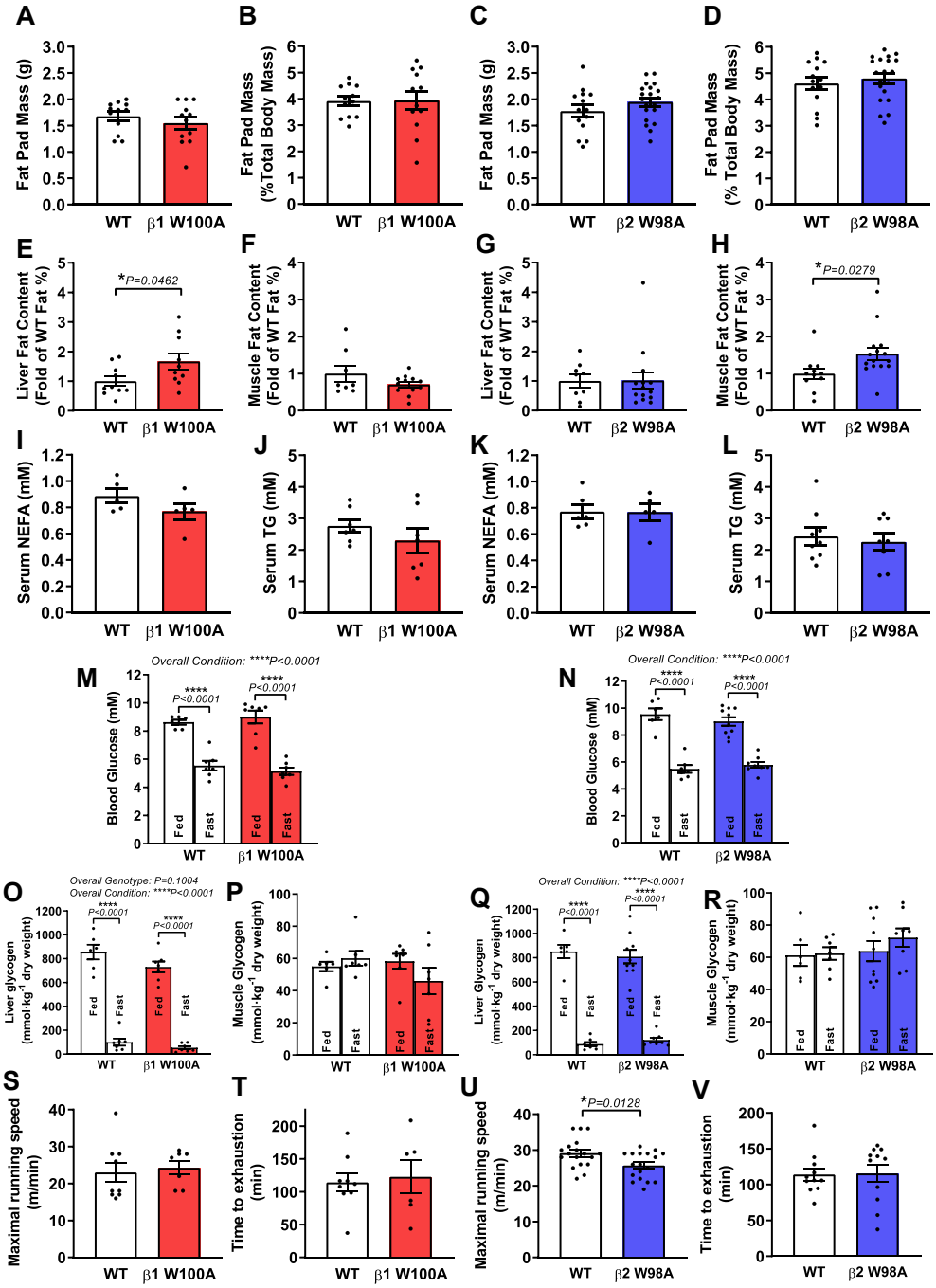

Figure 3: Loss of glycogen-bound AMPK β1 and β2 increases liver and skeletal muscle ectopic fat deposition independent of changes in fat pad mass, tissue glycogen or serum lipids. Tissues and serum were collected from male age-matched WT and KI mice (ranging from 14 to 32 wk). Epididymal fat pad (**A**) absolute mass and (**B**) mass relative to total body mass were determined in WT and β1 W100A mice (n = 12). Epididymal fat pad (**C**) absolute mass and (**D**) mass relative to total body mass were determined in WT and β2 W98A mice (n = 14–20). Freshly isolated (**E**) liver and (**F**) quadriceps muscle (n = 10 and n = 8–12, respectively) from WT and β1 W100A mice, and (**G**) liver and (**H**) muscle (n = 9–14 and n = 11–15, respectively) from WT and β2 W98A mice were subjected to EchoMRI. Following 6-h fast, colorimetric assays were used to determine serum (**I**) NEFA and (**J**) TG concentration (n = 7 and n = 5, respectively) in WT and β1 W100A and (**K**) NEFA and (**L**) TG concentration (n = 8–9 and n = 5–6, respectively) in WT and β2 W98A mice. (**M**) Blood glucose was measured, and glycogen content was determined using enzymatic analysis of (**O**) liver and (**P**) gastrocnemius muscle from fed or overnight fasted WT and W100A (n = 6–7). (**N**) Blood glucose and (**Q**) liver and (**R**) gastrocnemius muscle glycogen content are shown from fed or overnight fasted WT and β2 W98A mice (n = 6–10). Following treadmill acclimatisation, maximal running speed was determined in respective WT and (**S**) β1 W100A (n = 7–9) or (**U**) β2 W98A (n = 18) age-matched male mice (12–15 wk). Following 2–3 days' rest, time to exhaustion at 70% maximal speed was determined in respective WT and (**T**) β1 W100A (n = 6–9) or (**V**) β2 W98A (n = 11) mice. See also Figure S3. Data are represented as mean ± SEM; $*P < 0.05$; $****P < 0.0001$.

revealed no individual genotype differences during either the dark cycle, light cycle or cumulative 24 h period between activity levels (Figure 2E–F), food intake (Figure 2G–H), RER (Figure 2I–J) or patterns of whole-body fuel utilisation (Figure 2K–N) in β1 W100A, β2 W98A and respective WT mice.

3.4. Loss of glycogen-bound AMPK β1 and β2 increases liver and skeletal muscle ectopic fat content independent of changes in fat pad mass or serum lipids

To investigate potential differences in fat storage and availability, tissues and serum were collected in the fed and fasted states, respectively. Neither absolute (Figure 3A,C) nor epididymal fat pad mass relative to total body mass (Figure 3B,D) was different between respective WT and β1 W100A or β2 W98A mice. Considering liver and skeletal muscle as the major glycogen-storing tissues and the differential expression patterns of AMPK β1 and β2 isoforms in liver and skeletal muscle, respectively, fat content was next assessed in these tissues. Hepatic fat content was increased by 66% in β1 W100A relative to WT mice ($P = 0.0462$; Figure 3E), with no differences observed in skeletal muscle (Figure 3F). This was associated with reduced absolute β1 W100A liver mass ($P = 0.0257$; Supplementary Fig 2). In contrast, while β2 W98A liver fat content (Figure 3G) and absolute liver mass (Supplementary Fig 2) were similar to WT, skeletal muscle fat content was increased by 54% in β2 W98A versus WT mice ($P = 0.0279$; Figure 3H).

Serum analyses to investigate tissue fat availability revealed no changes in NEFA (Figure 3I,K) and TG (Figure 3J and 3l) concentrations in KI versus respective WT mice. Immunoblot analyses of fat uptake and oxidation machinery revealed that neither fatty acid transporter content (i.e., CPT1a [liver] and CPT1b [muscle]; Supplementary Fig 3) nor markers of mitochondrial content (i.e., VDAC, citrate synthase, OXPHOS complexes; Supplementary Fig 3) were altered in β1 W100A liver or β2 W98A muscle relative to respective WT tissues.

3.5. Disrupting AMPK β2 glycogen binding reduces maximal running speed

We next examined whether disrupting AMPK-glycogen binding affects tissue glycogen storage and utilisation and/or has functional consequences on maximal and sub-maximal treadmill running capacity. Overnight fasting reduced blood glucose ($P < 0.0001$; Figure 3M–N) and liver glycogen ($P < 0.0001$; Figure 3O,Q) in all WT and KI lines relative to the fed state (overall condition effects $P < 0.0001$). Fed and fasted levels of blood glucose (Figure 3M–N), liver glycogen (Figure 3O,Q) and skeletal muscle glycogen (Figure 3P,R) were not different in either β1 W100A or β2 W98A KI mice relative to respective WT. Despite an observed trend toward an overall genotype effect for reduced β1 W100A fed and fasting liver glycogen versus WT ($P = 0.1004$; Figure 3O), this did not reach statistical significance. β1 W100A mice displayed no change in maximal running speed or time to exhaustion during submaximal exercise (Figure 3S–T). However, β2 W98A mice had reduced maximal running speed ($P = 0.0128$; Figure 3U) despite similar submaximal exercise time to exhaustion (Figure 3V) relative to WT.

3.6. AMPK protein and kinase activity are reduced in liver and skeletal muscle of AMPK KI mice

To determine how loss of glycogen binding influences AMPK functionality in primary glycogen-storing tissues, phosphorylation status and total protein content of AMPK α, AMPK β and the established AMPK substrate acetyl-CoA carboxylase (ACC) were first assessed in livers from fed and fasted WT and β1 W100A mice (Figure 4A) and skeletal muscle from rested and maximally exercised WT and β2 W98A mice (Figure 4B). Total cellular AMPK α and β1 subunit protein levels were reduced in fed and fasted β1 W100A livers ($P = 0.0009$ and $P = 0.0020$, respectively; Figure 4C–D) versus WT (overall genotype effect $P < 0.0001$). An overall condition effect for decreased AMPK β1 upon fasting was also observed ($P = 0.0217$; Figure 4D). No differences in rested and exercised AMPK α and β2 subunit protein levels were detected in β2 W98A muscle relative to WT (Figure 4E–F), despite an overall genotype effect for reduced AMPK β2 in β2 W98A ($P = 0.0128$; Figure 4F) relative to WT. In adipose tissue, AMPK α and β1 subunit protein levels were similar between WT and β1 W100A mice (Supplementary Fig 4). Adipose tissue AMPK β2 levels were reduced 54% in β2 W98A mice versus WT ($P = 0.0055$), with no differences observed in adipose tissue AMPK α (Supplementary Fig 4). Reduced liver and muscle AMPK protein levels were associated with respective decreases in *Prkab1* and *Prkab2* gene expression in β1 W100A liver ($P = 0.0360$) and β2 W98A muscle ($P = 0.0150$) versus WT (Supplementary Fig 4).

Phosphorylated AMPK T172 (Figure 4G,I), ACC S79 (Figure 4H,J) or GS S641 (Figure 4K,M) relative to total protein were similar between fed and fasted β1 W100A and WT liver and between rested and exercised β2 W98A and WT muscle. An overall genotype effect of decreased liver AMPK T172 phosphorylation was observed in β1 W100A versus WT ($P = 0.0002$; Supplementary Fig 4), as well as an overall condition effect of increased exercise-induced muscle ACC S79 phosphorylation versus rest ($P = 0.0083$; Supplementary Fig 4). While trends were observed for overall condition effects of increased muscle exercise-induced AMPK T172 phosphorylation ($P = 0.0626$; Supplementary Fig 4), ACC S79 phosphorylation relative to total protein ($P = 0.1063$; Figure 4J) and an overall genotype effect of increased muscle GS S641 phosphorylation in β2 W98A versus WT ($P = 0.0986$; Supplementary Fig 4), these overall effects did not reach statistical significance. Consistent with a lack of change in the phosphorylation state of downstream targets relative to total protein in both genotypes, no changes in adenylate energy charge (i.e., AMP, ADP and ATP ratio) were observed in β1 W100A liver (Figure 4L) or β2 W98A muscle (Figure 4N) versus WT.

To determine the functional impact of reduced AMPK content in β1 W100A liver and β2 W98A muscle, kinase activity assays were performed using endogenous AMPK α IP from each tissue. An overall condition effect of increased liver AMPK α activity was observed following fasting ($P = 0.0103$; Figure 4Q). Total AMPK α activity in WT livers was increased by 32% following fasting ($P = 0.0206$; Figure 4Q); however, post-hoc testing revealed no fasting-induced increase in β1 W100A livers ($P > 0.9999$; Figure 4Q). There was a trend toward an overall genotype and condition interaction ($P = 0.0690$), but this failed to reach statistical significance (Figure 4Q). Total AMPK α activity was reduced 74% in fed ($P < 0.0001$) and 68% ($P < 0.0001$) in fasted β1 W100A livers relative to WT (overall genotype effect $P < 0.0001$; Figure 4Q,O top panel) and reduced 56% in resting β2 W98A muscle ($P = 0.0029$; Figure 4S,P top panel) versus WT with equal lysate input protein in the IP. When input AMPK from β1 W100A livers and β2 W98A muscle was increased to balance AMPK levels to those observed in WT tissues, an overall condition effect of increased AMPK α-specific activity was observed following fasting ($P = 0.0007$; Figure 4R). AMPK α-specific activity in WT liver was increased by 50% following fasting ($P = 0.0111$; Figure 4R,O bottom panel); however, post-hoc testing revealed no fasting-induced increase ($P = 0.3459$) in β1 W100A livers (overall genotype effect $P = 0.0479$; Figure 4R,O bottom panel). AMPK α-specific activity levels were similar between fed WT and β1 W100A livers (Figure 4R), and resting AMPK α-specific activity was also

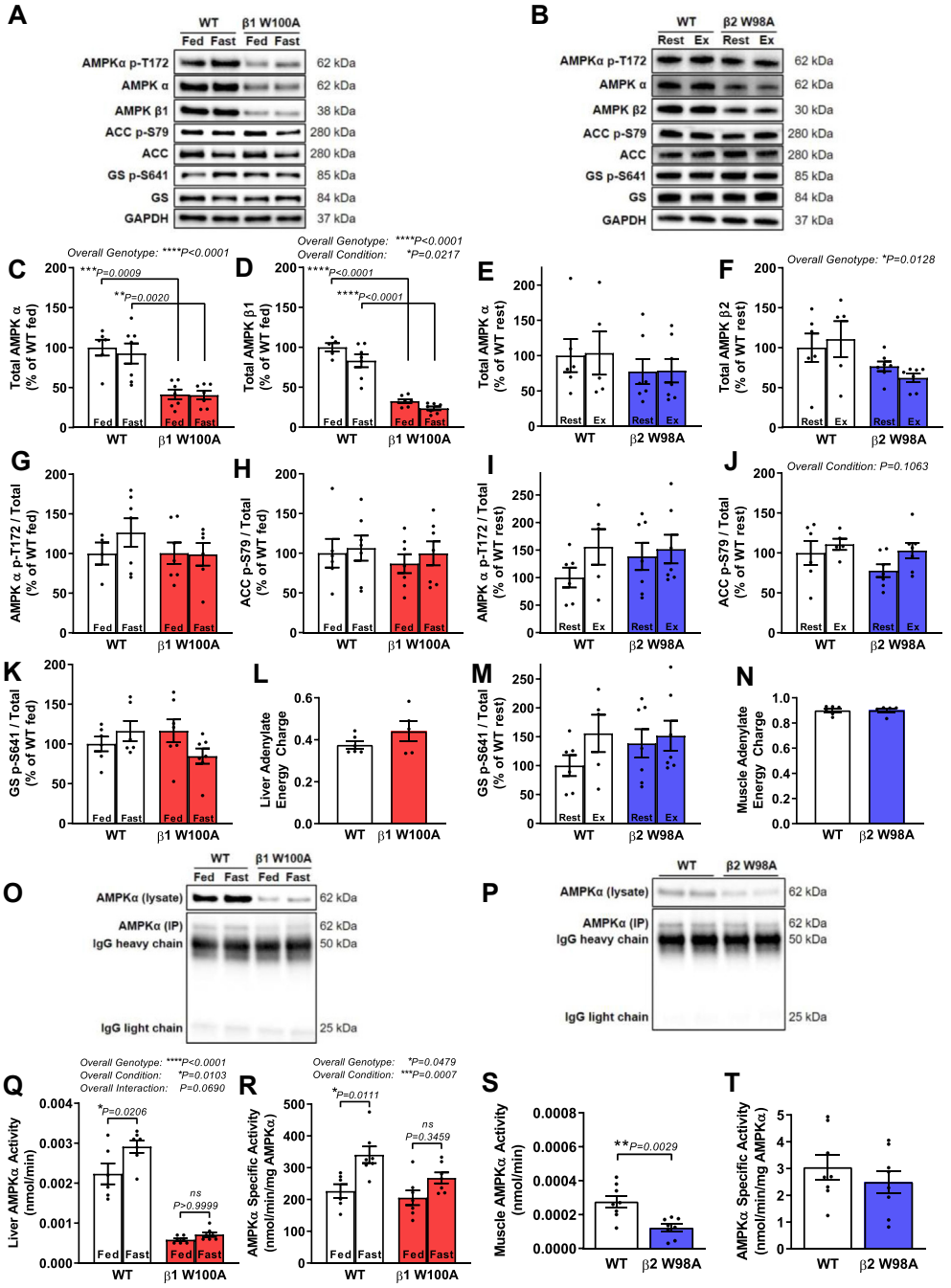

Figure 4: AMPK protein and kinase activity are reduced in liver and skeletal muscle of AMPK KI mice. Tissues were collected from male age-matched WT and KI mice (ranging from 12 to 22 wk; 14–32 wk for adenylate energy charge measurements). Representative immunoblots processed in parallel are shown for respective WT versus (**A**) fed and fasted β1 W100A liver or (**B**) gastrocnemius muscle from β2 W98A rested or treadmill exercised to exhaustion at 5° incline. Quantified immunoblots for total AMPK (**C**) α and (**D**) β from WT and β1 W100A liver (n = 4–7) and total AMPK (**E**) α and (**F**) β from WT and β2 W98A gastrocnemius muscle (n = 5–7) are shown. Quantified ratios of phosphorylated (**G**) AMPK T172, (**H**) ACC S79 and (**K**) GS S641 from fed and fasted WT and β1 W100A liver (n = 4–7), and phosphorylated (**I**) AMPK T172, (**J**) ACC S79 and (**M**) GS S641 from WT and β2 W98A gastrocnemius muscle (n = 5–7) relative to total protein are shown. Adenylate energy charge was determined via mass spectrometry analysis of AMP, ADP and ATP from respective WT and (**L**) β1 W100A liver (n = 5–6) or (**N**) β2 W98A gastrocnemius muscle (n = 5–6). Following AMPK α immunoprecipitation of respective WT and KI liver or muscle (**O–P top panels**, respectively; blots processed in parallel), total AMPK α activity was determined in (**Q**) fed and fasted β1 W100A liver (n = 6–7) and (**S**) rested β2 W98A gastrocnemius muscle via *in vitro* kinase assay using equal tissue input protein (n = 6–7). AMPK α-specific activity was determined in respective WT and (**R**) fed and fasted β1 W100A liver or (**T**) resting β2 W98A gastrocnemius muscle using balanced input of immunoprecipitated AMPK α determined from blots processed in parallel (**O–P bottom panels**; n = 6–7). See also Figure S4. Data are represented as mean ± SEM; $^{*}P < 0.05$; $^{**}P < 0.01$; $^{***}P < 0.001$; $^{****}P < 0.0001$.

normalised to WT levels in β2 W98A muscle (Figure 4T,P bottom panel).

4. DISCUSSION

Utilising unique AMPK β1 and β2 KI mouse models, we provide the first *in vivo* evidence of isoform-specific physiological roles of glycogen binding in the regulation of AMPK functionality and metabolism. The novel findings of this study include (a) increased adiposity, impaired whole-body glucose handling and reduced maximal running speed as a result of disrupting AMPK β2 glycogen binding; (b) ectopic fat accumulation in major glycogen-storing tissues liver and skeletal muscle induced by loss of glycogen-bound AMPK β1 and β2, respectively; and (c) reductions in total cellular AMPK that result in decreased total AMPK α activity in the liver and muscle and loss of fasting-induced liver total AMPK α and α-specific kinase activation *in vivo*. Collectively, our findings establish that AMPK-glycogen binding influences AMPK stability and metabolism *in vivo*.

Two whole-body AMPK KI mouse models were generated to target analogous residues within the AMPK β1 or β2 subunit CBM known to mediate glycogen binding [5,13,21] (Figure 1A). The AMPK β1 and β2 CBM are structurally similar; however, β2 CBM binding affinity is 4-fold higher for linear carbohydrates and up to 30-fold higher for single α 1,6-branched carbohydrates [22]. CBM binding affinity differences are due to an additional T101 residue in β2 that creates a pocket and accommodates this branching [23]. In line with previous structural, biochemical and microscopy-based evidence demonstrating AMPK and glycogen association *in vitro* [5,6,13,21,24], we show that full-length AMPK β1- and β2- containing heterotrimers associate with glycogen, and binding is disrupted with β1 W100A or β2 W98A KI mutation (Figure 1B).

A striking consequence of the AMPK β1 W100A and β2 W98A KI mutations is the observed reductions in total cellular AMPK relative to respective WT. The respective reductions in liver and muscle AMPK protein levels observed with β1 W100A and β2 W98A KI mutation are consistent with the observed destabilisation and rapid degradation of starch-binding domain-containing protein 1 (STBD1), a glycogen-binding protein recently shown to be a substrate of AMPK [25], in response to mutating a conserved tryptophan residue (W293) within its CBM. In light of these relevant findings demonstrating STBD1 degradation and reduced interaction with glycogen-associated proteins induced by CBM tryptophan mutation [26], our data suggest that AMPK β1 and β2 glycogen binding via their respective CBM may preserve an AMPK pool, potentially protecting AMPK from destabilisation and cellular degradation. While relative gene expression levels of *Prkab1* (AMPK β1) and *Prkab2* (AMPK β2) were also reduced in livers and muscle from KI compared to respective WT mice, respective AMPK β subunit proteins were translated and detectable with functional AMPK α kinase activity in tissues from each genotype. In the present study, transcriptional and/or translational regulatory mechanisms, including changes in mRNA processing, stability and translational efficiency, may contribute to the observed reductions in liver and muscle AMPK protein content in KI mice, in addition to potential post-translational changes in AMPK stability.

AMPK phosphorylates a repertoire of protein substrates residing in distinct organelles and subcellular compartments. Emerging evidence has demonstrated activation of different subcellular pools of AMPK that serve distinct subcellular roles in response to varying degrees of energy stress [27]. In the present study, liver fed/fasted and muscle rest/exercised levels of AMPK α T172 and ACC S79 phosphorylation relative to respective total protein content remain intact in KI mice despite reductions in liver and muscle AMPK α and/or β content relative to WT mice. These findings indicate that AMPK does not need to be glycogen-bound to interact with either the upstream kinases LKB1 and CaMKK2 or the unidentified T172 phosphatases. Our data showing lack of association between levels of AMPK protein/activity and ACC phosphorylation are contradictory to other reports from AMPK transgenic mouse models showing associated changes between phosphorylation of AMPK and ACC (e.g., [28—30]). However, these data are consistent with other reports demonstrating that T172 is dispensable for ACC S79 phosphorylation [19,31], intact ACC S79 phosphorylation despite siRNA-mediated knockdown of AMPK α and residual ACC S79 phosphorylation in the presence of kinase-dead AMPK α [32].

The AMPK β CBM interacts with the AMPK α subunit, forming the allosteric drug and metabolite (ADaM) site [33] and stabilising the α subunit kinase domain in its active formation [14,34], which can be destabilised when the CBM binds glycogen [14]. When AMPK input in IP was balanced to account for the observed reductions in AMPK content in KI tissues (Figure 4O,P, bottom panels), AMPK α-specific activity was normalised in both livers and muscle in the fed state. While increases in total AMPK α and α-specific activity were observed in the liver upon fasting (Figure 4Q—R), assessment of muscle from WT and β2 W98A mice at rest and following maximal treadmill exercise to exhaustion at a 5° incline revealed no exercise-induced increase in either total or specific AMPK activity. Therefore, AMPK kinase activity assays focused on analysing liver samples from fed and fasted β1 W100A mice versus WT, as well as resting muscle samples from β2 W98A mice versus WT. The observed loss of fasting-induced total and specific AMPK α activation as well as increased liver fat deposition observed in β1 W100A mice may indicate regulatory crosstalk between the glycogen-binding and ADaM sites in the allosteric control of *in vivo* AMPK activity. We speculate that a glycogen-bound AMPK "reserve pool" lost as a result of the CBM KI mutations is critical for suppressing cellular fat accumulation and maintaining cellular energy homeostasis in the liver and muscle. Impaired total and α-specific AMPK activation in the liver of β1 W100A mice may help explain liver fat accumulation, which has been shown to be reduced by AMPK activation *in vivo* [35]. In the context of increased muscle fat accumulation observed in high fat-fed mice with either muscle-specific deletion of AMPK α1 [36] or loss of AMPK's upstream kinase LKB1 in muscle [37], the observed increase in skeletal muscle fat content in chow-fed β2 W98A mice is potentially the consequence of reduced total AMPK activity and/or loss of a cellular AMPK pool(s) necessary for maintaining muscle lipid homeostasis.

The proposed *in vivo* energy-sensing role for AMPK-glycogen binding is supported by a series of *in vivo* studies demonstrating the ability of low skeletal muscle glycogen stores to increase AMPK catalytic activity in response to AICAR perfusion [9] and muscle contraction [10] in rats, as well as in humans at rest and during exercise [11,12]. Collectively, data from physiological studies suggest that β subunit CBMs act as sensors enabling AMPK to gauge cellular energy status (i.e., glycogen), increasing AMPK activity when stores are low and decreasing activity when stores are replete. Furthermore, *in vitro* findings have shown that AMPK is inhibited by glycogen and suggest that AMPK inhibition by glycogen's outer branch points exposed during glycogenolysis relieves AMPK's inhibition on GS to permit glycogen re-synthesis [13]. In contrast, data obtained from *in vivo* mouse models in the present study suggest that glycogen availability and AMPK-glycogen interaction elicit opposing actions on AMPK activity (i.e., low glycogen availability induced by fasting increases liver AMPK activity, and loss of glycogen binding induced by either β1 W100A or β2 W98A mutation decreases total AMPK α and/or α-specific activity). We hypothesise that this

difference may be due to residual glycogen-bound AMPK remaining under conditions of low liver glycogen availability in WT mice that is still capable of being activated upon fasting. In contrast, disruption of AMPK-glycogen binding in β1 W100A KI mice may result in complete loss of specific glycogen-bound AMPK pool(s) essential for fasting-induced liver AMPK activation.

Based on the novelty of the KI models, the present study focused on metabolic characterisation of chow-fed mice in the absence of any dietary intervention. While chow-fed β1 W100A mice displayed normal glucose and insulin tolerance, impaired glucose handling was observed in β2 W98A mice. These findings may be due to AMPK β2's predominant expression in skeletal muscle, a tissue responsible for the large majority (80–90%) of postprandial glucose disposal [38]. Impaired glucose handling observed in chow-fed β2 W98A mice versus WT in response to IPGTT performed relative to total body mass (Figure 1D) was associated with no changes in glucose-stimulated serum insulin levels (Figure 1K) but reduced muscle AMPK protein and total activity (Figure 4), suggesting a potential role for the glycogen-bound AMPK pool in maintaining *in vivo* muscle glucose transport. However, when glucose tolerance was examined in WT and β2 W98A mice in response to IPGTT performed relative to total lean mass (Figure 1L), impaired glucose handling was still observed in β2 W98A mice, suggesting that this impairment in glucose tolerance is not likely due to differences in lean body mass or muscle glucose disposal during insulin stimulation. It is worth noting that venous tail blood sampling was used to assess glucose homeostasis, in contrast to whole blood collected via retro-orbital bleeding to ensure sufficient sample volume for measurement of serum insulin and lipid concentrations. The lack of changes in glucose tolerance in β1 W100A mice and glucose intolerance observed in β2 W98A mice are consistent with IPGTT findings from AMPK α1 [39] and α2 [40] subunit whole-body knockout (KO) mice, respectively. In contrast, our findings of reduced glucose tolerance in β2 W98A mice fed a chow diet conflict with observations of reduced whole-body glucose tolerance in AMPK β2 KO mice [28,30] and transgenic mice expressing inactive AMPK α2 in skeletal muscle [41], which only display whole-body glucose intolerance following high fat feeding.

The increases in whole-body fat mass observed in β2 W98A mice and respective increases in liver and muscle ectopic fat deposition in β1 W100A and β2 W98A mice, associated with reduced AMPK protein and total kinase activity, are consistent with impaired AMPK regulation of anabolic and/or catabolic pathways [42]. Activation of the AMPK pathway becomes impaired during development of metabolic diseases, such as insulin resistance (IR) and type 2 diabetes [43], in which peripheral tissues including liver and muscle become infiltrated with ectopic fat [44]. Liver ectopic fat deposition is associated with hepatic steatosis and the development of non-alcoholic fatty liver disorder spectrum [45], and distinct patterns of ectopic fat deposition in liver and muscle coincide with the development of high-fat diet-induced IR in mice [46] and humans [44]. The overall lack of changes in metabolic cage measures, including physical activity, food intake and energy utilisation, observed in KI mice versus WT suggest these variables are unlikely to account for the observed increases in adiposity and/or ectopic fat. While there were no differences in adipose tissue AMPK protein levels in β1 W100A mice with similar levels of whole-body fat mass as WT mice, the observed reduction in AMPK β2 protein in adipose tissue from β2 W98A mice may contribute to their increased adiposity and muscle ectopic fat accumulation versus WT. Given that fat availability (i.e., serum lipids) and fat transporter content (i.e., tissue CPT1a or CPT1b) were not affected in either KI line versus respective WT, these data suggest a novel mechanism whereby glycogen binding may serve as an AMPK fuel-sensing "brake pedal" that inhibits de novo lipogenesis pathways and/or influences adipose mass-driven changes underlying liver and muscle ectopic fat accumulation.

The lack of changes in fed and fasting liver and skeletal muscle glycogen content suggests that the AMPK KI mutations do not directly influence tissue glycogen levels. In contrast to these KI models, reduced liver and muscle glycogen content was observed in mice lacking whole-body AMPK β2 [28,30], as well as reduced hepatic glycogen content and glycogenolysis rates observed in mice lacking AMPK α1 and α2 subunits in liver [29]. However, the functional impairment in maximal running speed observed in β2 W98A mice (Figure 3U) suggests potential effects of disrupting glycogen-bound AMPK on utilisation of muscle glycogen, which becomes the predominant fuel for skeletal muscle at higher exercise intensities (i.e., >80% of maximal O_2 uptake) [47]. This impaired maximal exercise capacity in β2 W98A mice is consistent with observations in mice lacking whole-body AMPK β2 [30] and skeletal muscle AMPK β1 and β2 [48]. We hypothesise that simultaneous disruption of both AMPK β1 and β2 glycogen binding in settings of energy stress (i.e., fasting, exercise) would elicit more pronounced metabolic effects on liver and muscle glycogen synthesis and/or glycogenolysis than single isoform KI mutations.

5. CONCLUSIONS

In summary, these data are the first to establish physiological consequences of disrupting AMPK-glycogen binding *in vivo*. Results from the present study demonstrate that loss of glycogen binding results in isoform-specific reductions in AMPK content and total AMPK α kinase activity in liver and muscle (β1 W100A and β2 W98A, respectively), as well as a reduction of AMPK content in adipose tissue (β2 W98A). This destabilisation of AMPK is associated with impaired whole-body glucose handling (β2 W98A), increased whole-body adiposity (β2 W98A), reduced maximal exercise capacity (β2 W98A) and increased ectopic fat deposition in liver and muscle (β1 W100A and β2 W98A, respectively). In addition, fasting-induced increases in total AMPK α and α-specific activity observed in WT liver were ablated in β1 W100A liver. AMPK binding to glycogen may therefore provide a critical reservoir of cellular AMPK required for liver, skeletal muscle and whole-body metabolic homeostasis that can be rapidly recruited upon the induction of metabolic stress and glycogenolysis. This glycogen-bound AMPK reservoir may be replenished upon glycogen repletion and restoration of energy homeostasis to help re-initiate cellular anabolic processes and potentially prevent deleterious effects of persistent AMPK activity including sustained blood glucose disposal. These insights into the effects of genetic loss of AMPK-glycogen binding lay the foundation for investigating the roles of glycogen-bound AMPK in physiological settings of energy stress, energy oversupply and the development of obesity and related metabolic diseases.

AUTHOR CONTRIBUTIONS

N.J.H., J.W., N.R.J., M.R.B., S.G., L.M.-S., W.J.S., N.X.Y.L and T.A.D. performed experiments and data analysis. N.J.H, J.W., N.R.J., M.R.B, S.G. and L.M.-S. assisted with mouse breeding, husbandry and tissue collections. B.E.K. and R.B. generated KI mouse models. N.J.H., J.W., S.G., J.W.S., J.S.O., R.B., B.E.K., and J.A.H. conceptualised the study and provided intellectual input. N.J.H, S.G., B.E.K. and J.A.H. provided financial support. N.J.H. wrote the manuscript, and all authors edited and approved the final version.

DATA AND MATERIALS AVAILABILITY

This article and its Supplementary Information files include all datasets generated during this study. All raw data are available from the Corresponding Author upon reasonable request. All unique biological materials generated and used in this study will be made available from the corresponding author upon reasonable request.

ACKNOWLEDGEMENTS

This work was supported by an Australian Catholic University Research Funding (ACURF) Early Career Researcher Grant awarded to N.J.H. (2016000348), National Health and Medical Research Council of Australia (NHMRC) project grant (1085460) awarded to B.E.K and S.G., and NHMRC Fellowship to B.E.K. (1078752). We thank the Mouse Engineering Garvan/ABR (MEGA) Facility and St. Vincent's BioResources Centre staff for their assistance with mouse generation and husbandry, respectively, and Fawzan Dinnunhan for assistance with gene expression analysis. This study utilised the Australian Phenomics Network Histopathology and Organ Pathology Service, University of Melbourne.

CONFLICT OF INTEREST

None declared.

APPENDIX A. SUPPLEMENTARY DATA

Supplementary data to this article can be found online at https://doi.org/10.1016/j.molmet.2020.101048.

REFERENCES

[1] Efeyan, A., Comb, W.C., Sabatini, D.M., 2015. Nutrient-sensing mechanisms and pathways. Nature 517(7534):302—310.

[2] Xiao, B., Heath, R., Saiu, P., Leiper, F.C., Leone, P., Jing, C., et al., 2007. Structural basis for AMP binding to mammalian AMP-activated protein kinase. Nature 449(7161):496—500.

[3] Scott, J.W., Hawley, S.A., Green, K.A., Anis, M., Stewart, G., Scullion, G.A., et al., 2004. CBS domains form energy-sensing modules whose binding of adenosine ligands is disrupted by disease mutations. Journal of Clinical Investigation 113(2):274—284.

[4] Townley, R., Shapiro, L., 2007. Crystal structures of the adenylate sensor from fission yeast AMP-activated protein kinase. Science 315(5819):1726—1729.

[5] Polekhina, G., Gupta, A., Michell, B.J., van Denderen, B., Murthy, S., Feil, S.C., et al., 2003. AMPK beta subunit targets metabolic stress sensing to glycogen. Current Biology 13(10):867—871.

[6] Hudson, E.R., Pan, D.A., James, J., Lucocq, J.M., Hawley, S.A., Green, K.A., et al., 2003. A novel domain in AMP-activated protein kinase causes glycogen storage bodies similar to those seen in hereditary cardiac arrhythmias. Current Biology 13(10):861—866.

[7] Wu, J., Puppala, D., Feng, X., Monetti, M., Lapworth, A.L., Geoghegan, K.F., 2013. Chemoproteomic analysis of intertissue and interspecies isoform diversity of AMP-activated protein kinase (AMPK). Journal of Biological Chemistry 288(50):35904—35912.

[8] Janzen, N.R., Whitfield, J., Hoffman, N.J., 2018. Interactive roles for AMPK and glycogen from cellular energy sensing to exercise metabolism. International Journal of Molecular Sciences 19(11).

[9] Wojtaszewski, J.F., Jorgensen, S.B., Hellsten, Y., Hardie, D.G., Richter, E.A., 2002. Glycogen-dependent effects of 5-aminoimidazole-4-carboxamide (AICA)-riboside on AMP-activated protein kinase and glycogen synthase activities in rat skeletal muscle. Diabetes 51(2):284—292.

[10] Derave, W., Ai, H., Ihlemann, J., Witters, L.A., Kristiansen, S., Richter, E.A., et al., 2000. Dissociation of AMP-activated protein kinase activation and glucose transport in contracting slow-twitch muscle. Diabetes 49(8):1281—1287.

[11] Wojtaszewski, J.F., MacDonald, C., Nielsen, J.N., Hellsten, Y., Hardie, D.G., Kemp, B.E., et al., 2003. Regulation of 5'AMP-activated protein kinase activity and substrate utilization in exercising human skeletal muscle. American Journal of Physiology. Endocrinology and Metabolism 284(4):E813—E822.

[12] Yeo, W.K., Lessard, S.J., Chen, Z.P., Garnham, A.P., Burke, L.M., Rivas, D.A., et al., 2008. Fat adaptation followed by carbohydrate restoration increases AMPK activity in skeletal muscle from trained humans. Journal of Applied Physiology (1985) 105(5):1519—1526.

[13] McBride, A., Ghilagaber, S., Nikolaev, A., Hardie, D.G., 2009. The glycogen-binding domain on the AMPK beta subunit allows the kinase to act as a glycogen sensor. Cell Metabolism 9(1):23—34.

[14] Li, X., Wang, L., Zhou, X.E., Ke, J., de Waal, P.W., Gu, X., et al., 2015. Structural basis of AMPK regulation by adenine nucleotides and glycogen. Cell Research 25(1):50—66.

[15] Yang, H., Wang, H., Jaenisch, R., 2014. Generating genetically modified mice using CRISPR/Cas-mediated genome engineering. Nature Protocols 9(8):1956—1968.

[16] Bergmeyer, H.U., 1974. Methods of enzymatic analysis, 2d English ed. New York, USA: Verlag Chemie; Academic Press.

[17] Peronnet, F., Massicotte, D., 1991. Table of nonprotein respiratory quotient: an update. Canadian Journal of Sport Sciences 16(1):23—29.

[18] Scott, J.W., Galic, S., Graham, K.L., Foitzik, R., Ling, N.X., Dite, T.A., et al., 2015. Inhibition of AMP-activated protein kinase at the allosteric drug-binding site promotes islet insulin release. Chemistry & Biology 22(6):705—711.

[19] Dite, T.A., Ling, N.X.Y., Scott, J.W., Hoque, A., Galic, S., Parker, B.L., et al., 2017. The autophagy initiator ULK1 sensitizes AMPK to allosteric drugs. Nature Communications 8(1):571.

[20] Hamilton, S.R., Stapleton, D., O'Donnell Jr., J.B., Kung, J.T., Dalal, S.R., Kemp, B.E., et al., 2001. An activating mutation in the gamma1 subunit of the AMP-activated protein kinase. FEBS Letters 500(3):163—168.

[21] Polekhina, G., Gupta, A., van Denderen, B.J., Feil, S.C., Kemp, B.E., Stapleton, D., et al., 2005. Structural basis for glycogen recognition by AMP-activated protein kinase. Structure 13(10):1453—1462.

[22] Koay, A., Woodcroft, B., Petrie, E.J., Yue, H., Emanuelle, S., Bieri, M., et al., 2010. AMPK beta subunits display isoform specific affinities for carbohydrates. FEBS Letters 584(15):3499—3503.

[23] Mobbs, J.I., Koay, A., Di Paolo, A., Bieri, M., Petrie, E.J., Gorman, M.A., et al., 2015. Determinants of oligosaccharide specificity of the carbohydrate-binding modules of AMP-activated protein kinase. Biochemical Journal 468(2):245—257.

[24] Bendayan, M., Londono, I., Kemp, B.E., Hardie, G.D., Ruderman, N., Prentki, M., 2009. Association of AMP-activated protein kinase subunits with glycogen particles as revealed in situ by immunoelectron microscopy. Journal of Histochemistry and Cytochemistry 57(10):963—971.

[25] Ducommun, S., Deak, M., Zeigerer, A., Goransson, O., Seitz, S., Collodet, C., et al., 2019. Chemical genetic screen identifies Gapex-5/GAPVD1 and STBD1 as novel AMPK substrates. Cellular Signalling 57:45—57.

[26] Zhu, Y., Zhang, M., Kelly, A.R., Cheng, A., 2014. The carbohydrate-binding domain of overexpressed STBD1 is important for its stability and protein-protein interactions. Bioscience Reports 34(4).

[27] Zong, Y., Zhang, C.S., Li, M., Wang, W., Wang, Z., Hawley, S.A., et al., 2019. Hierarchical activation of compartmentalized pools of AMPK depends on severity of nutrient or energy stress. Cell Research 29(6):460—473.

[28] Dasgupta, B., Ju, J.S., Sasaki, Y., Liu, X., Jung, S.R., Higashida, K., et al., 2012. The AMPK beta2 subunit is required for energy homeostasis during metabolic stress. Molecular and Cellular Biology 32(14):2837—2848.

[29] Hughey, C.C., James, F.D., Bracy, D.P., Donahue, E.P., Young, J.D., Viollet, B., et al., 2017. Loss of hepatic AMP-activated protein kinase impedes the rate of glycogenolysis but not gluconeogenic fluxes in exercising mice. Journal of Biological Chemistry 292(49):20125–20140.

[30] Steinberg, G.R., O'Neill, H.M., Dzamko, N.L., Galic, S., Naim, T., Koopman, R., et al., 2010. Whole body deletion of AMP-activated protein kinase {beta}2 reduces muscle AMPK activity and exercise capacity. Journal of Biological Chemistry 285(48):37198–37209.

[31] Scott, J.W., Ling, N., Issa, S.M., Dite, T.A., O'Brien, M.T., Chen, Z.P., et al., 2014. Small molecule drug A-769662 and AMP synergistically activate naive AMPK independent of upstream kinase signaling. Chemistry & Biology 21(5): 619–627.

[32] Hoffman, N.J., Parker, B.L., Chaudhuri, R., Fisher-Wellman, K.H., Kleinert, M., Humphrey, S.J., et al., 2015. Global phosphoproteomic analysis of human skeletal muscle reveals a Network of exercise-regulated kinases and AMPK substrates. Cell Metabolism 22(5):922–935.

[33] Langendorf, C.G., Oakhill, J.S., Kemp, B.E., 2018. Visualizing AMPK drug binding sites through crystallization of full-length phosphorylated alpha2beta1gamma1 heterotrimer. Methods in Molecular Biology 1732:15–27.

[34] Xiao, B., Sanders, M.J., Carmena, D., Bright, N.J., Haire, L.F., Underwood, E., et al., 2013. Structural basis of AMPK regulation by small molecule activators. Nature Communications 4:3017.

[35] Foretz, M., Even, P.C., Viollet, B., 2018. AMPK activation reduces hepatic lipid content by increasing fat oxidation in vivo. International Journal of Molecular Sciences 19(9).

[36] Wu, W., Xu, Z., Zhang, L., Liu, J., Feng, J., Wang, X., et al., 2017. Muscle-specific deletion of Prkaa1 enhances skeletal muscle lipid accumulation in mice fed a high-fat diet. Journal of Physiology & Biochemistry.

[37] Shan, T., Zhang, P., Bi, P., Kuang, S., 2015. Lkb1 deletion promotes ectopic lipid accumulation in muscle progenitor cells and mature muscles. Journal of Cellular Physiology 230(5):1033–1041.

[38] DeFronzo, R.A., Tripathy, D., 2009. Skeletal muscle insulin resistance is the primary defect in type 2 diabetes. Diabetes Care 32(Suppl 2):S157–S163.

[39] Viollet, B., Andreelli, F., Jorgensen, S.B., Perrin, C., Flamez, D., Mu, J., et al., 2003. Physiological role of AMP-activated protein kinase (AMPK): insights from knockout mouse models. Biochemical Society Transactions 31(Pt 1):216–219.

[40] Viollet, B., Andreelli, F., Jorgensen, S.B., Perrin, C., Geloen, A., Flamez, D., et al., 2003. The AMP-activated protein kinase alpha2 catalytic subunit controls whole-body insulin sensitivity. Journal of Clinical Investigation 111(1):91–98.

[41] Fujii, N., Ho, R.C., Manabe, Y., Jessen, N., Toyoda, T., Holland, W.L., et al., 2008. Ablation of AMP-activated protein kinase alpha2 activity exacerbates insulin resistance induced by high-fat feeding of mice. Diabetes 57(11):2958–2966.

[42] Grahame Hardie, D., 2014. AMP-activated protein kinase: a key regulator of energy balance with many roles in human disease. Journal of Internal Medicine 276(6):543–559.

[43] Ruderman, N.B., Carling, D., Prentki, M., Cacicedo, J.M., 2013. AMPK, insulin resistance, and the metabolic syndrome. Journal of Clinical Investigation 123(7):2764–2772.

[44] Shulman, G.I., 2014. Ectopic fat in insulin resistance, dyslipidemia, and cardiometabolic disease. New England Journal of Medicine 371(12):1131–1141.

[45] Farrell, G.C., Larter, C.Z., 2006. Nonalcoholic fatty liver disease: from steatosis to cirrhosis. Hepatology 43(2 Suppl 1):S99–S112.

[46] Turner, N., Kowalski, G.M., Leslie, S.J., Risis, S., Yang, C., Lee-Young, R.S., et al., 2013. Distinct patterns of tissue-specific lipid accumulation during the induction of insulin resistance in mice by high-fat feeding. Diabetologia 56(7): 1638–1648.

[47] van Loon, L.J., Greenhaff, P.L., Constantin-Teodosiu, D., Saris, W.H., Wagenmakers, A.J., 2001. The effects of increasing exercise intensity on muscle fuel utilisation in humans. The Journal of Physiology 536(Pt 1):295–304.

[48] O'Neill, H.M., Maarbjerg, S.J., Crane, J.D., Jeppesen, J., Jorgensen, S.B., Schertzer, J.D., et al., 2011. AMP-activated protein kinase (AMPK) beta1beta2 muscle null mice reveal an essential role for AMPK in maintaining mitochondrial content and glucose uptake during exercise. Proceedings of the National Academy of Sciences of the U S A 108(38):16092–16097.

Author/s:
Hoffman, NJ; Whitfield, J; Janzen, NR; Belhaj, MR; Galic, S; Murray-Segal, L; Smiles, WJ; Ling, NXY; Dite, TA; Scott, JW; Oakhill, JS; Brink, R; Kemp, BE; Hawley, JA

Title:
Genetic loss of AMPK-glycogen binding destabilises AMPK and disrupts metabolism

Date:
2020-11-01

Citation:
Hoffman, N. J., Whitfield, J., Janzen, N. R., Belhaj, M. R., Galic, S., Murray-Segal, L., Smiles, W. J., Ling, N. X. Y., Dite, T. A., Scott, J. W., Oakhill, J. S., Brink, R., Kemp, B. E. & Hawley, J. A. (2020). Genetic loss of AMPK-glycogen binding destabilises AMPK and disrupts metabolism. MOLECULAR METABOLISM, 41, https://doi.org/10.1016/j.molmet.2020.101048.

Persistent Link:
http://hdl.handle.net/11343/271813

File Description:
Published version